

NLTE carbon abundance determination in selected A- and B-type stars and the interpretation of C I emission lines

S. A. Alexeeva,¹ T. A. Ryabchikova,¹ & L. I. Mashonkina¹

¹Institute of Astronomy of the Russian Academy of Sciences

48 Pyatnitskaya St. 119017, Moscow, Russia

Released 2014 Xxxxx XX

ABSTRACT

We constructed a comprehensive model atom for C I – C II using the most up-to-date atomic data available and evaluated the non-local thermodynamic equilibrium (NLTE) line formation for C I and C II in classical 1D models representing the atmospheres of A and late B-type stars. Our NLTE calculations predict the emission that appears at effective temperature of 9250 to 10 500 K depending on $\log g$ in the C I 8335, 9405 Å singlet lines and at $T_{\text{eff}} > 15\,000$ K ($\log g = 4$) in the C I 9061 – 9111 Å, 9603 – 9658 Å triplet lines. A prerequisite of the emission phenomenon is the overionization-recombination mechanism resulting in a depopulation of the lower levels of C I to a greater extent than the upper levels. Extra depopulation of the lower levels of the transitions corresponding to the near-infrared lines, is caused by photon loss in the UV lines C I 2479, 1930, and 1657 Å. We analysed the lines of C I and C II in Vega, HD 73666, Sirius, 21 Peg, π Cet, HD 22136, and ι Her taking advantage of their observed high-resolution spectra. The C I emission lines were detected in the four hottest stars, and they were well reproduced in our NLTE calculations. For each star, the mean NLTE abundances from lines of the two ionization stages, C I and C II, including the C I emission lines, were found to be consistent. We show that the predicted C I emission phenomenon depends strongly on whether accurate or approximate electron-impact excitation rates are applied.

Key words: line: formation, stars: abundances

1 INTRODUCTION

Rapid development of observational techniques over the last decade has resulted in dramatic improvement of the quality of spectral observations in astronomy. Thanks to Echelle spectrographs, we are able to cover wide spectral regions with one exposure, obtaining spectra with a high spectral resolution of up to $R = \lambda/\Delta\lambda = 120\,000$ and high signal-to-noise ratio. Huge amounts of high quality spectra are collected in different archives with the open access for the astronomical community. High quality spectra require immediately an adequate improvement in theoretical methods of spectrum analysis, model atmospheres, line formation scenarios, etc.

Fossati et al. (2009) studied three apparently normal A and B sharp-lined stars and found the C I emission lines at 8335, and 9406 Å in the hottest of them, π Cet. The absorption C I lines in the 7111–7120 Å range are rather shallow and allow us to determine only an upper limit for the abundance. In local thermodynamic equilibrium (LTE) analysis, π Cet reveals a disparity between C I and C II, in line

with Roby & Lambert (1990). For the cooler star, 21 Peg, Fossati et al. (2009) could not obtain consistent abundances from different C I lines, namely the abundances obtained from C I 4932, 5052, 5380 Å were found to be significantly smaller than those from other C I lines.

Fossati et al. (2009) discussed several mechanisms of the C I emission in π Cet. Emission lines may form, if the star has a chromosphere, however, there is no evidence for chromospheric activity in π Cet. This star was classified as a Herbig Ae/Be star due to small infrared (IR) excess (Malfait et al. 1998), suggesting the existence of a circumstellar disc. This is supported by detection of an emission signature in H_{α} (Fossati et al. 2009). However, half-widths of the C I emission lines do not differ from those of the C I absorption lines, giving evidence for their common origin in the star’s atmosphere. Fossati et al. (2009) proposed that the emission can be caused by the departures from LTE in the C I line formation. In the literature there are examples of successfully reproducing the observed emission lines by non-local thermodynamic equilibrium (NLTE) calculations,

arXiv:1607.07672v1 [astro-ph.SR] 26 Jul 2016

for example, Mg I 12 μm in the Sun (Carlsson et al. 1992), Mn II 6122–6132 \AA in the three late type B stars (Sigut 2001), C II 6151, 6462 \AA in τ Sco (B0V) and C II 6462 \AA in HR 1861 (B1V) (Nieva & Przybilla 2008).

There are few NLTE studies of C I/C II in the early A to late B stars. Rentzsch-Holm (1996) computed a negative and small absolute value of less than 0.05 dex NLTE abundance corrections for lines of C II in A-type stars. Przybilla et al. (2001) obtained very small NLTE corrections for the C I and C II lines in the visible region using a Vega model atmosphere with an effective temperature $T_{\text{eff}} = 9550$ K. The NLTE carbon abundance analysis of 20 sharp-lined early B stars in the effective temperature range of 16000–33000 K, including two stars with $T_{\text{eff}} < 18000$ K, was performed by Nieva & Przybilla (2012). None of the carbon NLTE papers investigated the NLTE effects for the C I near-IR lines in the early A to late B stars.

This paper aims to understand mechanism(s) of the C I emission in B-type stars and to treat the method of accurate abundance determination from different lines of C I and C II based on NLTE line formation. We construct a comprehensive model atom for C I – C II using the most up-to-date atomic data available so far and analyse lines of C I and C II in high-resolution spectra of reference A and B-type stars with well-determined stellar parameters.

The paper is organized as follows. Section 2 describes an updated model atom of C I–C II and discusses departures from LTE for C I – C II in the model atmospheres of A–B stars and mechanisms driving the C I emission lines. In Sect. 3, we analyse the C I near-IR emission lines observed in the four B-type stars and determine the C abundance of the selected A–B stars. We inspect the abundance differences between different lines of a common species and between two ionisation stages, C I and C II. Our conclusions are summarized in Sect. 4.

2 NLTE LINE FORMATION FOR C I–C II

2.1 Model atom and atomic data

Alexeeva & Mashonkina (2015) developed and described in detail the carbon model atom that represents the term structure of C I well and only approximately that of C II. Here, the model atom was updated by extending the C II term structure and including recent accurate collisional data for C I.

Energy levels of C II. Energy levels of C II belong to the doublet terms of the $2s^2 nl$ ($n = 2 - 10$, $l = 0 - 2$), $2s^2 nf$ ($n = 4 - 10$), $2s^2 ng$ ($n = 5 - 10$), $2s^2 2p nh$ ($n = 6 - 10$), $2s2p^3$, and $2s2p 3l$ ($l = 0 - 1$) electronic configurations and the quartet terms of $2s2p^2$, $2s2p^3$, $2p^3$, $2s2p 3l$ ($l = 0 - 3$). We thus include explicitly the C II energy levels up to 0.01 eV below the ionization threshold. Fine structure splitting was taken into account everywhere, up to $n = 5$. All the C II states with $n = 11$ to 13 have close together energies, therefore they were combined into superlevels. Energy levels were adopted from the NIST¹ database (Ralchenko et al. 2008). The term diagram for C II is shown in Fig. 1.

Radiative data. We included 2138 allowed bound–bound ($b - b$) transitions, whose transition probabilities were taken from the NIST and VALD (Kupka et al. 1999) databases, where available, and the Opacity Project (OP) database TOPbase² (Cunto et al. 1993, Luo et al. 1989, Hibbert et al. 1993). Their Photo-ionization cross-sections for levels of C II with $n \leq 10$, $l \leq 3$ are from TOPbase, and we adopted the hydrogen-like cross-sections for the higher excitation levels.

Collisional data. For all the transitions between levels of the C I $2p^2$, $2p^3$, $2p3l$ ($l = 0, 1, 2$), and $2p4s$ electronic configurations we use the effective collision strengths computed by Wang et al. (2013) on the base of the B -spline R -matrix with pseudo states method. For the transitions involving the higher excitation levels of the $2p4p$, $2p4d$, and $2p5s$ electronic configurations we adopted cross-sections calculated by Reid (1994) in the close-coupling approximation using the R -matrix method. For the transitions connecting the 30 lowest levels in C II we use the effective collision strengths from Wilson et al. (2005). The remaining transitions in both C I and C II were treated using an approximation formula of van Regemorter (1962) for the allowed transitions and assuming the effective collision strength $\Omega_{ij} = 1$ for the forbidden transitions. Ionization by electronic collisions was everywhere treated through the Seaton (1962) classical path approximation.

2.2 Method of calculations

We used the code DETAIL (Butler & Giddings 1985) based on the accelerated Λ -iteration method (Rybicki & Hummer 1991) for solving the radiative transfer and statistical equilibrium (SE) equations. The opacity package was updated by Przybilla et al. (2011). The departure coefficients, $b_i = n_{\text{NLTE}} / n_{\text{LTE}}$, were then used to calculate the synthetic NLTE line profiles via the BINMAG3 code (Kochukhov 2010) and SYNTHV-NLTE code (Ryabchikova et al. 2016). Here, n_{NLTE} and n_{LTE} are the SE and thermal (Saha–Boltzmann) number densities, respectively.

We used plane-parallel (1D), chemically homogeneous model atmospheres calculated with the LLMODELS code (Shulyak et al. 2004). An exception is Sirius, for which we took the Kurucz’s model³ computed with the atmospheric parameters close to those derived by Hill & Landstreet (1993).

The carbon abundance was determined from line profile fitting. The uncertainty in fitting the observed profile is less than 0.02 dex for weak lines and 0.03 dex for strong lines.

2.3 SE of carbon

In Fig. 2, we show the LTE and NLTE fractions of C I, C II, and C III in the model atmospheres of different temperatures. In each model, C II dominates the total element abundance throughout the line-formation region. The fraction of C I everywhere does not exceed several thousandth parts, and in the line-formation layers, it is smaller in NLTE than in LTE due to ultraviolet (UV) overionization.

¹ <http://physics.nist.gov/PhysRefData/>

² <http://legacy.gsfc.nasa.gov/topbase>

³ <http://kurucz.harvard.edu/stars/SIRIUS/ap04t9850g43k0he05y.dat>

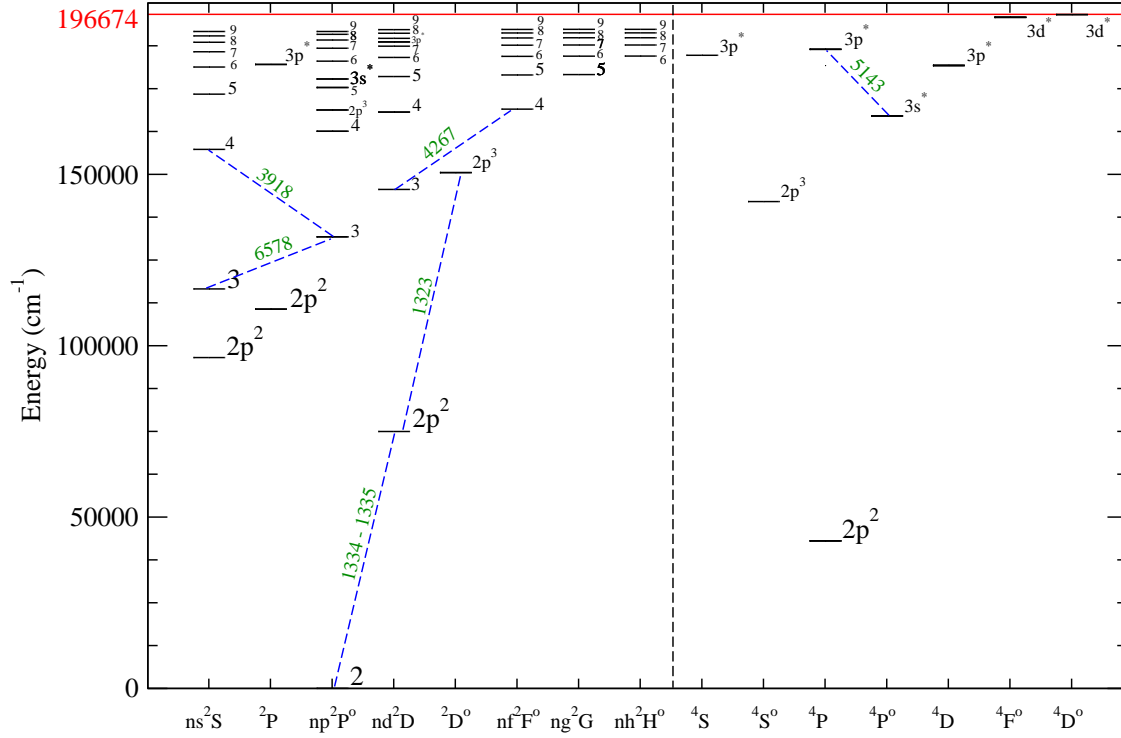


Figure 1. The term diagram for singly-ionized carbon. The dashed lines indicate the seven transitions, where the investigated spectral lines arise.

Fig. 3 displays a behaviour of the departure coefficients for selected levels in the model atmospheres with $T_{\text{eff}} / \log g / [\text{Fe}/\text{H}] = 10400 / 3.5 / 0$ and $17500 / 3.8 / 0$. Deep in the atmosphere, the departure coefficients are equal to unity because of a dominance of the collision processes in establishing the statistical equilibrium. In the line-formation layers, outward $\log \tau_{5000} = 0.5$, NLTE leads to depleted populations of the C I levels because of UV overionization.

The deviations from LTE are small everywhere for the ground state of C II. In the model 10400/3.5/0, outwards $\log \tau_{5000} = -0.5$, the C II high-excitation levels $3p^2P^\circ$, $4s^2S$, and $4p^2P^\circ$ are overpopulated via the UV radiative pumping transitions $2p^2\ ^2D - 3p^2P^\circ$ (C II 1760 Å), $3p^2P^\circ - 4s^2S$ (C II 3918 Å), and $2p^2\ ^2D - 4p^2P^\circ$ (C II 1142 Å). In the model 17500/3.8/0, these UV lines form in higher atmospheric layers, around $\log \tau_{5000} = -1.0$, resulting in a depopulation of the upper levels via spontaneous transitions.

The NLTE effects for a given spectral line can be understood from analysis of the departure coefficients of the lower and upper levels, b_l and b_u , at the line formation depths. The line can be strengthened or weakened compared with its LTE strength depending on the b_l and b_u values. Here, we consider two lines with similar excitation energy of the lower level, E_{exc} , but different gf values. Atomic data for the investigated lines are indicated in Table 1. In the model 10400/3.5/0, the C I 5052 Å line ($3s^1P^\circ - 4p^1D$) is weak and it forms in the layers around $\log \tau_{5000} = 0$, where $b_l < 1$ and $b_l < b_u$. NLTE leads to weakening this line and positive NLTE abundance correction of $\Delta_{\text{NLTE}} = \log \epsilon_{\text{NLTE}} - \log \epsilon_{\text{LTE}} = +0.45$ dex. In contrast, C I 9111 Å ($3s^3P^\circ - 3p^3P$) is strong and its core forms around $\log \tau_{5000} = -1.2$, where $b_l > b_u$ and the line source function drops below the *Planck*

function resulting in strengthened line and negative NLTE abundance correction of $\Delta_{\text{NLTE}} = -0.13$.

2.4 Mechanisms driving the C I emission

Our calculations predict that the C I near-IR lines at 8335 Å ($3s^1P^\circ - 3p^1S$), 9405 Å ($3s^1P^\circ - 3p^1D$), 9061–9111 Å ($3s^3P^\circ - 3p^3P$), and 9603–9658 Å ($3s^3P^\circ - 3p^3S$) may appear as emission lines depending on the atmospheric parameters.

The C I 8335 and 9405 Å singlet lines reveal an emission at the lower effective temperature compared with the triplet lines. The lower $\log g$, the lower T_{eff} is, at which the emission profile is developed for given line. Fig. 4 shows how a variation in T_{eff} and $\log g$ affects theoretical profiles of C I 9405, 9658, and 9088 Å and at which atmospheric parameters the line absorption changes to emission. For example, the C I 9405 Å emission line appears at $9250 \text{ K} < T_{\text{eff}} < 9500 \text{ K}$ in the $\log g = 2$ models and at $T_{\text{eff}} > 10500 \text{ K}$ when $\log g = 4$. In contrast, the triplet line at 9658 Å comes into emission at $T_{\text{eff}} > 15000 \text{ K}$ in the $\log g = 4$ models. Having appeared at specific $T_{\text{eff}}/\log g$, the emission is strengthened towards higher temperature, reaches its maximum and gradually disappears. For example, in the models with $\log g = 3$, the strongest emission in C I 9405 Å is predicted for $T_{\text{eff}} = 16000 \text{ K}$, and it almost disappears at $T_{\text{eff}} = 22000 \text{ K}$ (Fig. 5).

Which processes in C I do drive the emission in the IR lines? How do they depend on atmospheric parameters? In Fig. 6, we present the NET rates, $\text{NET} = n_l(R_{lu} + C_{lu}) - n_u(R_{ul} + C_{ul})$, in the model 10400/3.5/0 at $\log \tau_{5000} = -1.3$, where the C I 8335 and 9405 Å emission form (Fig. 3). Here, R_{lu} and C_{lu} are radiative and collisional rates, respectively,

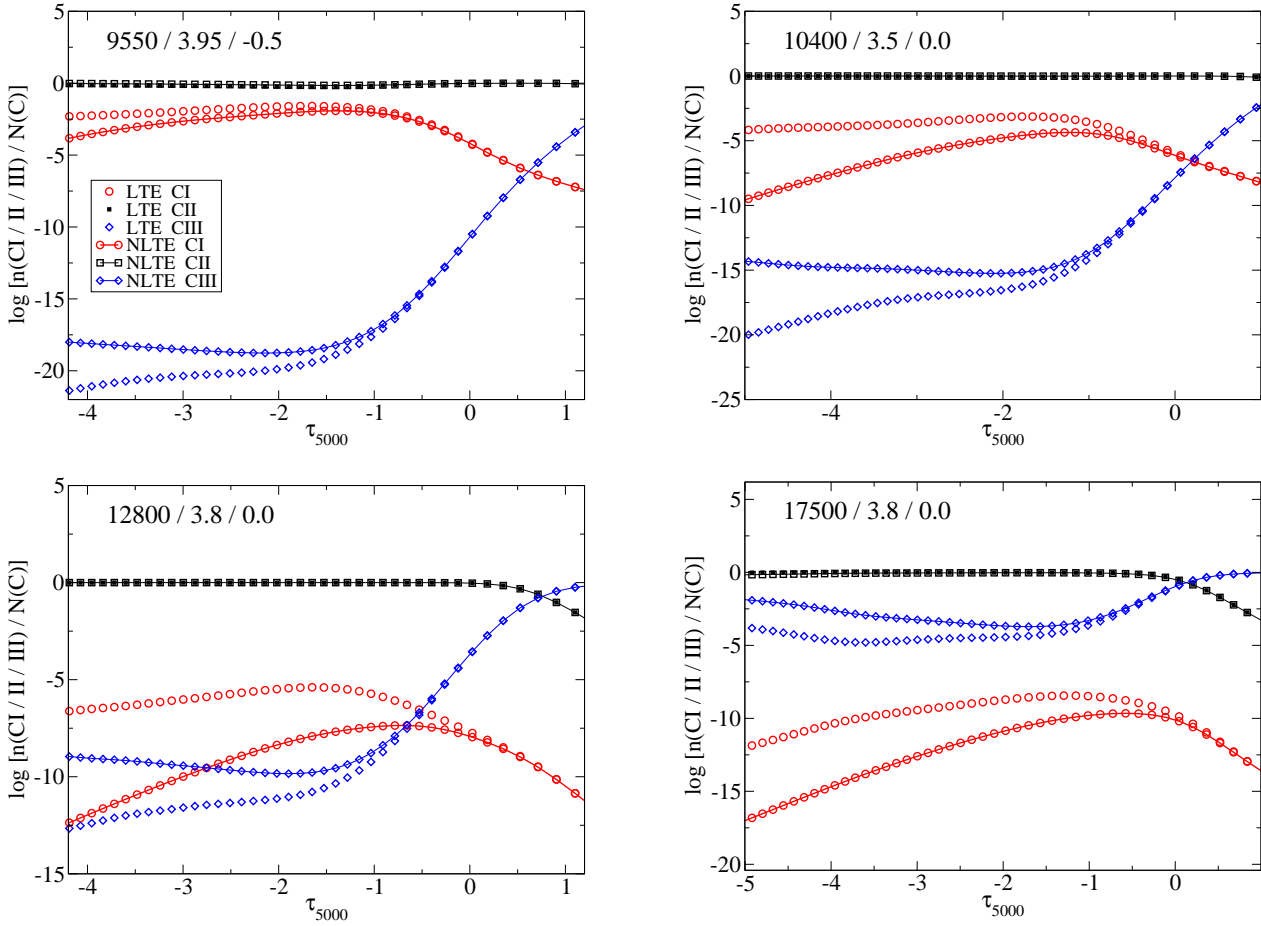


Figure 2. NLTE and LTE fractions of C I, C II, and C III in the model atmospheres of different effective temperature.

for the transition from low to upper level, and R_{ul} and C_{ul} for the inverse transition. The high-excitation levels, with $E_{\text{exc}} > 7.9$ eV, including the upper levels of the investigated transitions, are mainly populated by recombination from C II that follows an overionization of the C I ground state ($\text{NET} = 2 \cdot 10^{10} \text{ s}^{-1} \text{ cm}^{-3}$) and low-excitation levels, including the lower levels of the investigated transitions (NET varies between $1 \cdot 10^{10} \text{ s}^{-1} \text{ cm}^{-3}$ and $1 \cdot 10^{11} \text{ s}^{-1} \text{ cm}^{-3}$). Thus, the overionization-recombination mechanism resulting in a depopulation of the lower levels to a greater extent than the upper levels is a prerequisite of the emission phenomenon. Extra depopulation of the levels $3s^1P^\circ$ and $3s^3P^\circ$ can be caused by photon loss in the UV transitions $2p^2 \ ^1S - 3s^1P^\circ$ (2479 Å), $2p^2 \ ^1D - 3s^1P^\circ$ (1930 Å), and $2p^2 \ ^3P - 3s^3P^\circ$ (1657 Å). An influence of these UV transitions on the SE of C I in the layers, where the IR lines form, depends on atmospheric parameters. In the model 10400/3.5/0, photon loss in C I 2479 Å drains population of $3s^1P^\circ$ effectively in the layers around $\log \tau_{5000} = -1.3$, with $\text{NET} = 5 \cdot 10^{10} \text{ s}^{-1} \text{ cm}^{-3}$, while the transitions corresponding to C I 1930 Å and 1657 Å are in detailed balance because of $\tau_{1930} \gg 1$ and $\tau_{1657} \gg 1$. We performed test calculations by reducing a radiative rate of C I 2479 Å by 10%. This resulted in weakened emission, such that the line centre relative flux of C I 9405 Å reduced from 1.053 to 1.028.

With increasing T_{eff} , optical depth of formation of the

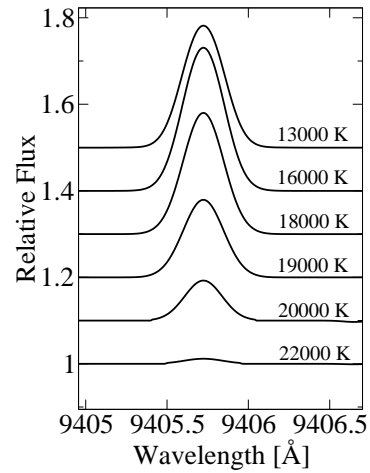


Figure 5. Changes in the C I 9405 Å line profile with temperature increasing. Everywhere, $\log g = 3$, $[\text{C}/\text{Fe}] = 0$, $V \sin i = 0 \text{ km s}^{-1}$, and $\xi_t = 1 \text{ km s}^{-1}$. The theoretical spectra are convolved with an instrumental profile of $R = 65000$.

C I UV lines shift inwards (Fig. 3 for $T_{\text{eff}} = 17500 \text{ K}$) and photon losses depopulate not only $3s^1P^\circ$, but also $3s^3P^\circ$, resulting in the emission triplet lines at 9061 – 9111 Å and 9603 – 9658 Å.

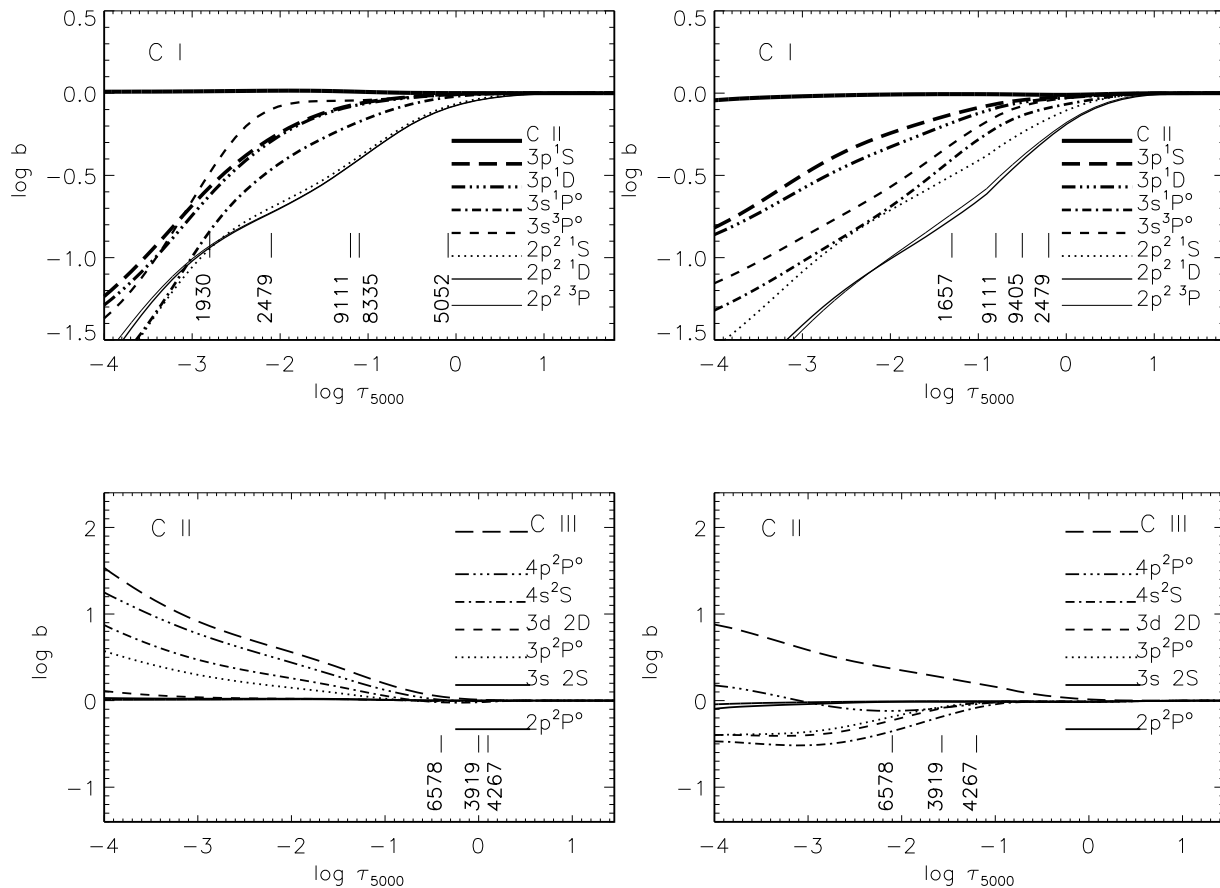


Figure 3. Departure coefficients for selected levels of C I (top row) and C II plus the C III ground state (bottom row) as a function of $\log \tau_{5000}$ in the model atmospheres 10400 / 3.5 / 0.0 (left-hand column) and 17500 / 3.8 / 0.0 (right-hand column). The wavelengths and vertical marks indicate the location of optical depth unity for the lines under consideration.

3 CARBON LINES IN THE SELECTED STARS

3.1 Stellar sample, observations, and atmospheric parameters

Our sample includes seven sharp-lined stars, with well-determined stellar parameters (Table 2). Due to low rotational velocities, with $V \sin i \lesssim 40 \text{ km s}^{-1}$, they allow spectral analysis to be done at the highest precision, maximizing the chance to identify even weak emission lines (WELs) in their spectra. They are either single stars, or primaries in close binary systems (SB1) with much fainter companions, or individual components in a visual binary.

For all the stars, the spectra in the visible spectral range (3690–10480 Å) were obtained with the Echelle SpectroPolarimetric Device for the Observation of Stars (ESPaDONs) attached at the 3.6 m telescope of the Canada–France–Hawaii Telescope (CFHT) observatory. Spectra were extracted from the ESPaDONs archive⁴. The resolving power and signal-to-noise ratio are $R = 65\,000$ and $S/N \simeq 500\text{--}600$, respectively. For Sirius, we also used the UV spectrum that covers the wavelength region between 1265 and 1368 Å.

It was obtained with the Goddard High Resolution Spectrograph on the *HubbleSpaceTelescope* (*HST*), and it has $R = 25\,000$ and S/N of 100–200, in general. Characteristics of the observed spectra for individual stars are given in Table 3.

We comment on the programme stars.

The star 21 Peg (HD 209459) is known from previous studies as a ‘normal’ single star with $V \sin i \sim 4 \text{ km s}^{-1}$ (Sadakane 1981, Fossati et al. 2009).

The star π Cet (HD 17081) is an SB1 star with $V \sin i \sim 20 \text{ km s}^{-1}$. The observed small infrared excess at $\lambda \lesssim 3 \mu$ makes it a candidate for Herbig Ae/Be star (Malfait et al. 1998). Since its spectrum is not visibly contaminated by the companion, it fully serves for our analysis. This star was already used by Smith & Dworetzky (1993) as a normal comparison star in the abundance study of chemically peculiar stars.

For 21 Peg and π Cet, their effective temperatures and surface gravities were spectroscopically determined from the Balmer lines (Fossati et al. 2009).

HD 22136 is also a normal star with $V \sin i \sim 15 \text{ km s}^{-1}$, showing no chemical peculiarities. Its fundamental parameters were derived by Bailey & Landstreet (2013) based on the Geneva and uvby β photometry.

Effective temperature and surface gravity of Vega

⁴ <http://www.cfht.hawaii.edu/Instruments/Spectroscopy/Espadons/>

Table 1. Lines of C I and C II used in abundance analysis.

λ , Å	Transition	$\log gf$	E_{exc} , eV	λ , Å	Transition	$\log gf$	E_{exc} , eV
C I				C I			
1329.09	$2p^2 \ ^3P_1 - 2p^3 \ ^3P_0^\circ$	-1.231	0.00	9094.83	$3s \ ^3P_2^\circ - 3p \ ^3P_2$	0.151	7.49
1329.10	$2p^2 \ ^3P_1 - 2p^3 \ ^3P_2^\circ$	-1.147	0.00	9111.80	$3s \ ^3P_2^\circ - 3p \ ^3P_1$	-0.297	7.49
1329.12	$2p^2 \ ^3P_1 - 2p^3 \ ^3P_1^\circ$	-1.355	0.00	9603.02	$3s \ ^3P_0^\circ - 3p \ ^3S_1$	-0.896	7.48
1329.59	$2p^2 \ ^3P_1 - 2p^3 \ ^3P_2^\circ$	-0.662	0.01	9658.43	$3s \ ^3P_2^\circ - 3p \ ^3S_1$	-0.280	7.49
1329.60	$2p^2 \ ^3P_1 - 2p^3 \ ^3P_2^\circ$	-1.136	0.01	10123.87	$3p \ ^1P_1 - 3d \ ^1P_1^\circ$	-0.03	8.54
1459.03	$2p^2 \ ^1D_2 - 3d \ ^1P_1^\circ$	-1.282	1.26	10691.24	$3s \ ^3P_2^\circ - 3p \ ^3D_3$	0.344	7.49
1463.34	$2p^2 \ ^1D_2 - 3d \ ^1F_3^\circ$	-0.396	1.26	10683.08	$3s \ ^3P_1^\circ - 3p \ ^3D_2$	0.08	7.48
1657.91	$2p^2 \ ^3P_1 - 3s \ ^3P_0^\circ$	-0.845	0.00	10685.36	$3s \ ^3P_0^\circ - 3p \ ^3D_1$	-0.27	7.48
1658.12	$2p^2 \ ^3P_2 - 3s \ ^3P_1^\circ$	-0.748	0.01	10729.53	$3s \ ^3P_2^\circ - 3p \ ^3D_2$	-0.42	7.49
4762.52	$3s \ ^3P_1^\circ - 4p \ ^3P_2$	-2.335	7.48	10707.32	$3s \ ^3P_1^\circ - 3p \ ^3D_1$	-0.41	7.48
4766.66	$3s \ ^3P_1^\circ - 4p \ ^3P_1$	-2.617	7.48	10753.98	$3s \ ^3P_2^\circ - 3p \ ^3D_1$	-1.60	7.49
4770.02	$3s \ ^3P_1^\circ - 4p \ ^3P_0$	-2.437	7.48	C II			
4771.73	$3s \ ^3P_2^\circ - 4p \ ^3P_2$	-1.866	7.49	1335.70	$2p \ ^2P_{3/2}^\circ - 2p^2 \ ^2D_{5/2}$	-0.335	0.01
4775.89	$3s \ ^3P_2^\circ - 4p \ ^3P_1$	-2.304	7.49	1323.86	$2p^2 \ ^2D_{5/2} - 2p^3 \ ^2D_{3/2}^\circ$	-1.284	9.29
4932.04	$3s \ ^1P_1^\circ - 4p \ ^1S_0$	-1.658	7.69	1323.91	$2p^2 \ ^2D_{3/2} - 2p^3 \ ^2D_{3/2}^\circ$	-0.337	9.29
5052.14	$3s \ ^1P_1^\circ - 4p \ ^1D_2$	-1.303	7.69	1323.95	$2p^2 \ ^2D_{5/2} - 2p^3 \ ^2D_{5/2}^\circ$	-0.144	9.29
5380.32	$3s \ ^1P_1^\circ - 4p \ ^1P_1$	-1.616	7.69	1324.00	$2p^2 \ ^2D_{3/2} - 2p^3 \ ^2D_{5/2}^\circ$	-1.288	9.29
6007.17	$3p \ ^3D_1 - 6s \ ^3P_1^\circ$	-2.062	8.64	3918.96	$3p \ ^2P_{1/2}^\circ - 4s \ ^2S_{1/2}$	-0.533	16.33
6012.22	$3p \ ^3D_1 - 5d \ ^3F_2^\circ$	-2.005	8.64	3920.68	$3p \ ^2P_{3/2}^\circ - 4s \ ^2S_{1/2}$	-0.232	16.33
6013.21	$3p \ ^3D_3 - 5d \ ^3F_4^\circ$	-1.314	8.65	4267.00	$3d \ ^2D_{3/2} - 4f \ ^2F_{5/2}^\circ$	0.563	18.05
6014.83	$3p \ ^3D_2 - 6s \ ^3P_1^\circ$	-1.584	8.64	4267.26	$3d \ ^2D_{5/2} - 4f \ ^2F_{7/2}^\circ$	0.716	18.05
6587.61	$3p \ ^1P_1 - 4d \ ^1P_1^\circ$	-1.003	8.54	4267.26	$3d \ ^2D_{5/2} - 4f \ ^2F_{5/2}^\circ$	-0.584	18.05
7111.46	$3p \ ^3D_1 - 4d \ ^3F_2^\circ$	-1.09	8.64	5132.95	$2p3s \ 4P_{1/2}^\circ - 2p3p \ 4P_{3/2}$	-0.211	20.70
7113.17	$3p \ ^3D_3 - 4d \ ^3F_4^\circ$	-0.77	8.65	5133.28	$2p3s \ 4P_{3/2}^\circ - 2p3p \ 4P_{5/2}$	-0.178	20.70
7115.17	$3p \ ^3D_2 - 4d \ ^3F_3^\circ$	-0.93	8.64	5137.25	$2p3s \ 4P_{1/2}^\circ - 2p3p \ 4P_{1/2}$	-0.911	20.70
7115.18	$3p \ ^3D_1 - 5s \ ^3P_0^\circ$	-1.47	8.64	5139.17	$2p3s \ 4P_{3/2}^\circ - 2p3p \ 4P_{3/2}$	-0.707	20.70
7116.98	$3p \ ^3D_3 - 5s \ ^3P_2^\circ$	-0.91	8.65	5143.49	$2p3s \ 4P_{3/2}^\circ - 2p3p \ 4P_{1/2}$	-0.212	20.70
7119.65	$3p \ ^3D_2 - 5s \ ^3P_1^\circ$	-1.148	8.64	5145.16	$2p3s \ 4P_{5/2}^\circ - 2p3p \ 4P_{5/2}$	0.189	20.71
8335.14	$3s \ ^1P_1^\circ - 3p \ ^1S_0$	-0.437	7.69	5151.09	$2p3s \ 4P_{5/2}^\circ - 2p3p \ 4P_{3/2}$	-0.179	20.71
9405.73	$3s \ ^1P_1^\circ - 3p \ ^1D_2$	0.286	7.69	6578.05	$3s \ ^2S_{1/2} - 3p \ ^2P_{3/2}^\circ$	-0.021	14.45
9061.43	$3s \ ^3P_1^\circ - 3p \ ^3P_2$	-0.347	7.48	6582.88	$3s \ ^2S_{1/2} - 3p \ ^2P_{1/2}^\circ$	-0.323	14.45
9062.49	$3s \ ^3P_0^\circ - 3p \ ^3P_1$	-0.455	7.48	7231.33	$3p \ ^2P_{1/2}^\circ - 3d \ ^2D_{3/2}$	0.039	16.33
9078.28	$3s \ ^3P_1^\circ - 3p \ ^3P_1$	-0.581	7.48	7236.41	$3p \ ^2P_{3/2}^\circ - 3d \ ^2D_{5/2}$	0.294	16.33
9088.51	$3s \ ^3P_1^\circ - 3p \ ^3P_0$	-0.43	7.48	7237.16	$3p \ ^2P_{3/2}^\circ - 3d \ ^2D_{3/2}$	-0.660	16.33

Table 2. Atmospheric parameters of the selected stars and sources of the data.

HD	Name	Sp. t.	T_{eff} (K)	$\log g$ (CGS)	[Fe/H]	ξ_t (km s ⁻¹)	$V \sin i$ (km s ⁻¹)	Ref.
17081	π Cet	B7 IV E	12800	3.8	0.0	0.5	20	1
22136	–	B8V C	12700	4.2	-0.28	1.1	15	2
48915	Sirius	A1V+DA	9850	4.3	0.4	1.8	16.5	3
73666	40 Cnc	A1V C	9382	3.78	0.16	1.9	10	4
160762	ι Her	B3 IV SPB	17500	3.8	0.02	1.0	6	5
172167	Vega	A0Va C	9550	3.95	-0.5	2.0	14	6
209459	21 Peg	B9.5V C	10400	3.5	0.0	0.5	4	1

References: 1 = Fossati et al. (2009); 2 = Bailey & Landstreet (2013); 3 = Hill & Landstreet (1993); 4 = Fossati et al. (2007); 5 = Nieva & Przybilla (2012); 6 = Przybilla et al. (2000).

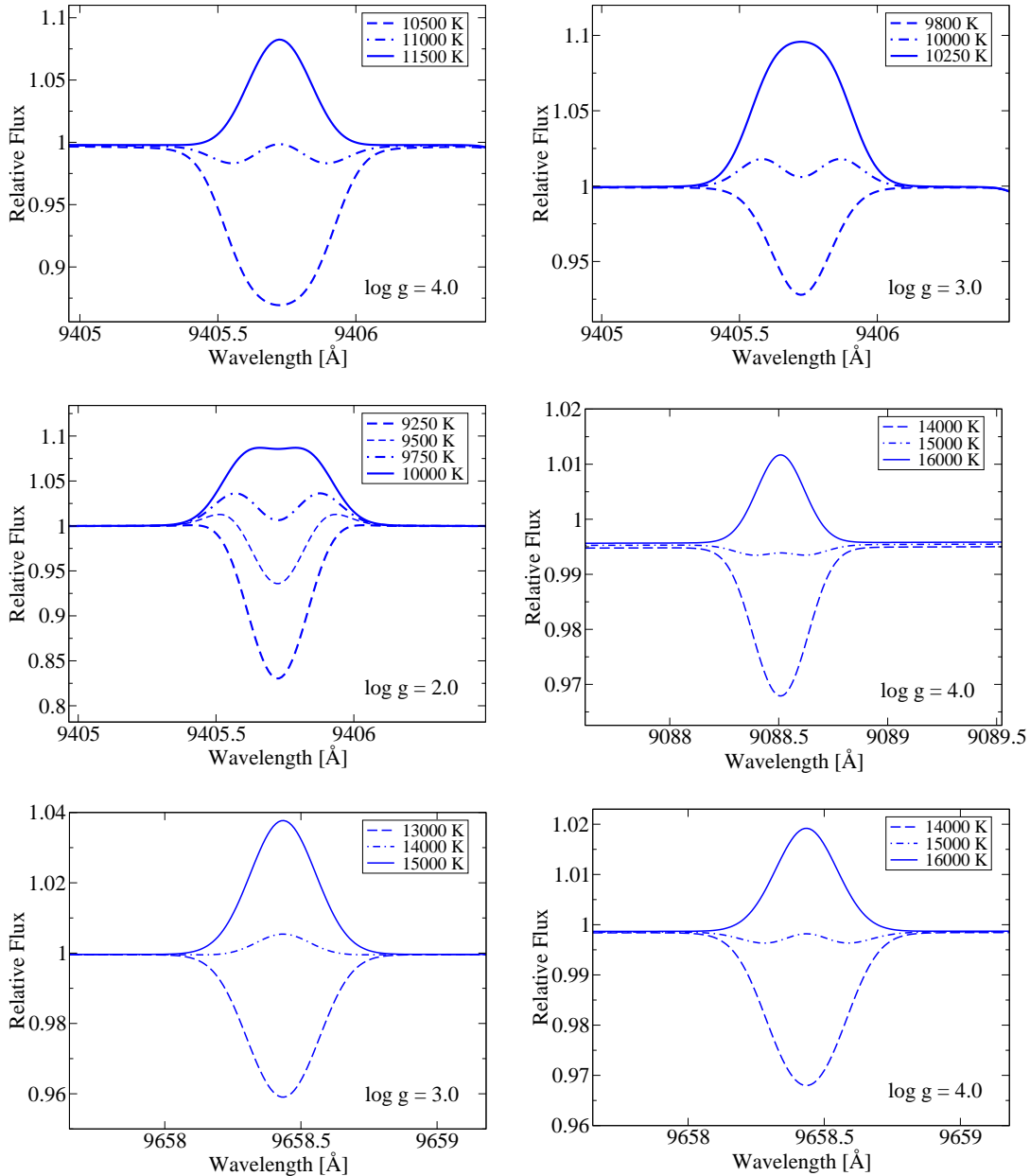


Figure 4. Change of the line profile with a variation in T_{eff} and $\log g$ for C I 9405 Å, 9658 Å, and 9088 Å. Everywhere, $[\text{C}/\text{Fe}] = 0$, $V \sin i = 0 \text{ km s}^{-1}$, and $\xi_t = 1 \text{ km s}^{-1}$. The theoretical spectra are convolved with an instrumental profile of $R = 65000$.

(HD 172167) were determined by Przybilla et al. (2000) from the Balmer line wings and Mg I and Mg II lines. Vega is a rapidly rotating star seen pole-on. Rapid rotation causes a change of the surface shape from spherical to ellipsoidal one, therefore, the temperature stratification and surface gravity vary from the pole to equator (Hill et al. 2010). We ignore the non-spherical effects in our study and analyse Vega’s flux spectrum using the average temperature and gravity. Vega was also classified as a mild λ Bootis-type star (Venn & Lambert 1990).

ι Her (HD 160762) is a single bright star, with $V \sin i \sim 6 \text{ km s}^{-1}$. Its atmospheric parameters were determined spectroscopically from all available H and He lines and multiple ionisation equilibria, and they were confirmed via the

spectral energy distribution and the *Hipparcos* distance (Nieva & Przybilla 2012).

HD 73666 is a Blue Straggler and a member of the Praesepe cluster. It is previously considered as an Ap (Si) star, but appears to have the abundances of a normal A-type star (Fossati et al. 2007). This star is a primary component of SB1, as is the case for many other Blue Stragglers (Leonard 1996). The flux coming from the secondary star is negligible, as previously checked by Burkhart & Coupry (1998), so the star was analysed ignoring the presence of the secondary. The physical parameters were taken from Fossati et al. (2007). Both Fe I excitation (for the effective temperature) and Fe I/Fe II ionisation (for $\log g$) equilibria were used in the parameter determination.

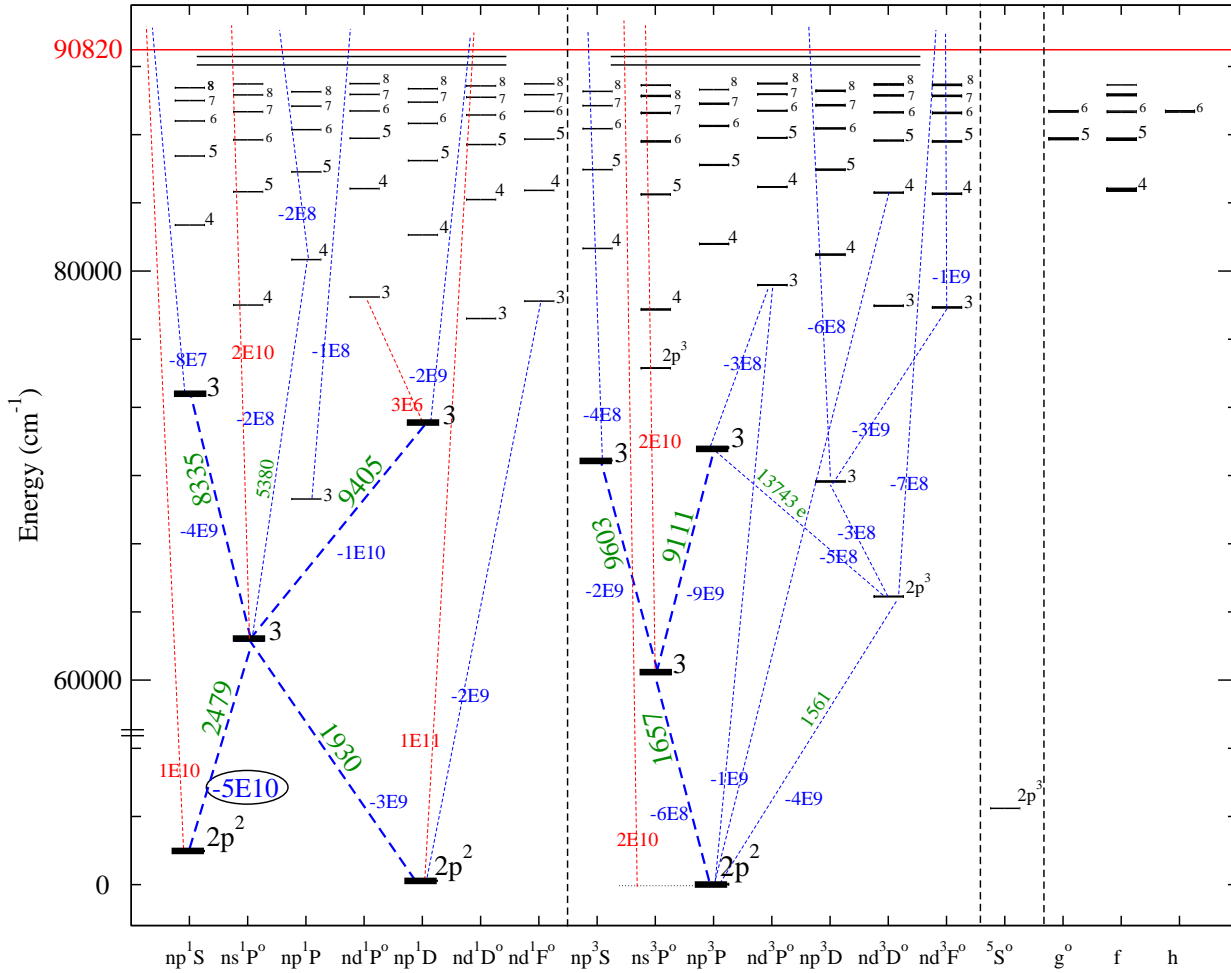


Figure 6. The NET-diagram at $\log\tau_{5000} = -1.3$ in the model 10400/3.5/0. Wavelengths (\AA) and NET values ($\text{s}^{-1} \text{cm}^{-3}$) are quoted for the selected transitions. NETs of negative sign are marked in blue, and positive marked in red (only on-line available).

Table 3. Characteristics of observed spectra.

HD	V ¹ (mag)	Telescope/ spectrograph	Spectral range (\AA)	t_{exp} (s)	Observing run year/month	R	S/N
17081	4.2	1	3690–10480	120	2005/02	65000	600
22136	6.9	1	3690–10480	356	2008/03	65000	500
48915	-1.5	1	3690–10480	0.6	2011/02	65000	500
		2	1265–1368	3482	1996/11	25000	200
73666	6.6	1	3690–10480	1600	2006/01	65000	660
160762	3.8	1	3690–10480	240	2012/06	65000	600
172167	0.0	1	3690–10480	8	2011/07	65000	500
209459	5.8	1	3690–10480	290	2013/08	65000	600

Notes. ¹ V is a visual magnitude from the SIMBAD database.

Telescope / spectrograph: 1 = CFHT/ESPaDOnS; 2 = HST/GHRS.

The Sirius binary system (HD 48915 = HIP 32349) is composed of a main sequence A1V star and a hot DA white dwarf. It is an astrometric visual binary system at a distance of only 2.64 pc. Their physical parameters are available with the highest precision and were taken from Hill & Landstreet (1993). Sirius A is classified as a hot metallic-line (Am) star.

3.2 Analysis of C I emission lines in B-type stars

Emission lines of C I were detected in the observed spectra of the four stars: 21 Peg, HD 22136, π Cet, and ι Her. In 21 Peg, HD 22136, and π Cet only C I 8335 and 9405 \AA are in emission, while the hottest star of our sample, ι Her, also has the emission lines at 9061–9111 \AA and 9603–9658 \AA . Some examples are shown in Fig. 7.

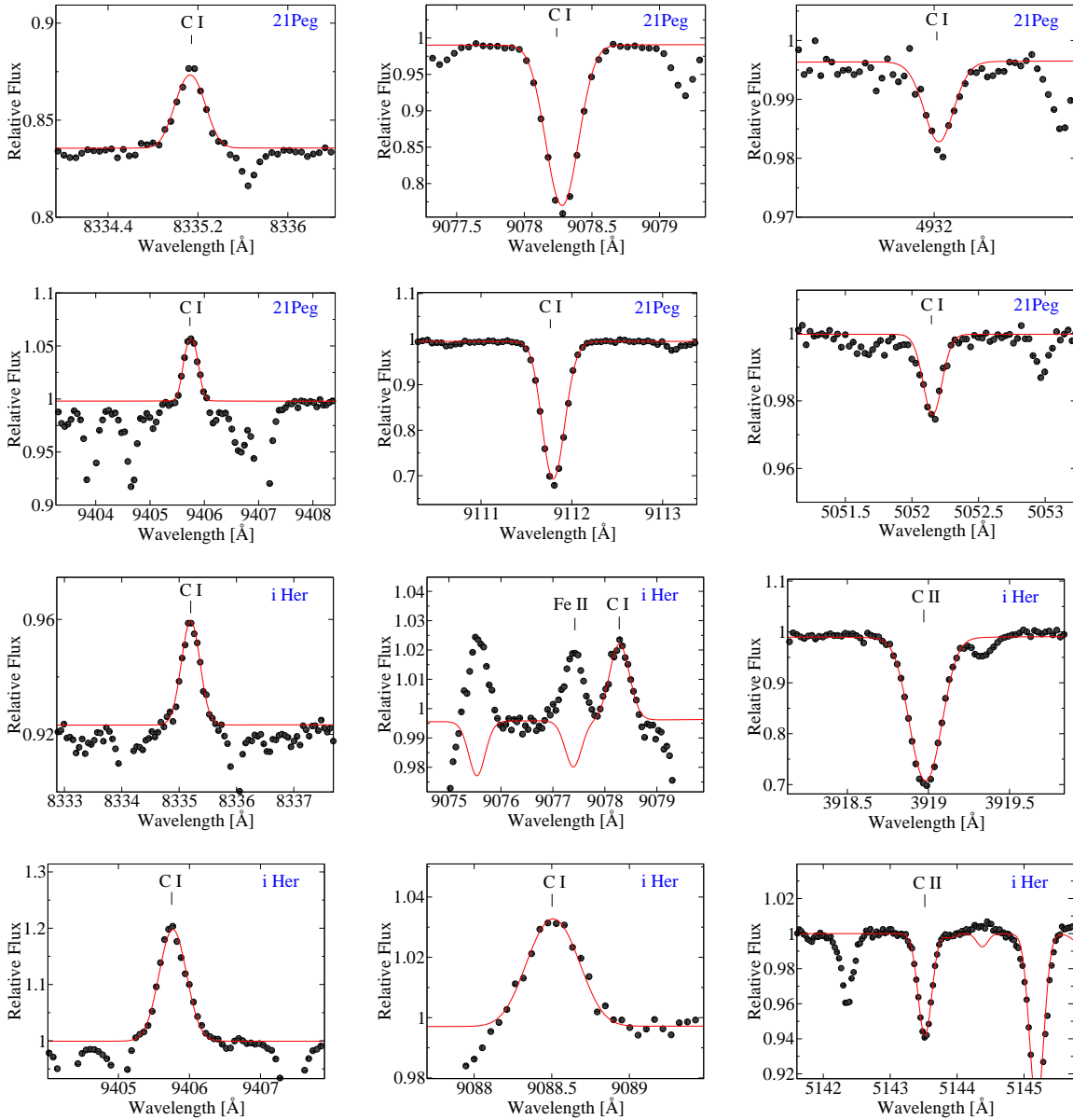


Figure 7. Best fits (solid curves) of the selected C I and C II lines in 21 Peg (two top rows) and ι Her (two bottom rows). The observed spectra are shown by bold dots.

For each star, our NLTE calculations reproduce well the observed C I emission lines, using the treated model atom of C I – C II and adopted atmospheric parameters. The best NLTE fits of the selected emission lines in 21 Peg and ι Her are presented in Fig. 7.

Analysis of stellar emission lines provides an opportunity to test collisional data for C I. As described in Sect. 2.1, electron-impact excitation data for C I were computed by Wang et al. (2013) and Reid (1994). We checked the influence of varying collisional rates on the appearance of the C I emission lines in the model 10400/3.5/0 representing the atmosphere of 21 Peg. Calculations were performed with the three different sets of data, namely (i) 703 transitions from Wang et al. (2013) plus 323 transitions from Reid (1994)

and plus formula of van Regemorter (1962) for the remaining transitions; this is our standard model as described in Sect. 2.1, (ii) 537 transitions from Reid (1994) and the formula of van Regemorter (1962) and $\Omega = 1$ for the remaining allowed and forbidden transitions, (iii) only the formula of van Regemorter (1962) and $\Omega = 1$ were employed. Fig. 8 shows that the effect on C I 9405 Å is large. With the theoretical approximations, we computed the absorption line profile, and this is not supported by observations of 21 Peg, where C I 9405 Å is in emission. Only applying accurate collisional rates allows us to obtain the emission. However, the emission is stronger in calculations with Reid (1994) than Wang et al. (2013) data. The choice was decided by comparison with C I 9405 Å observed in 21 Peg. With the ele-

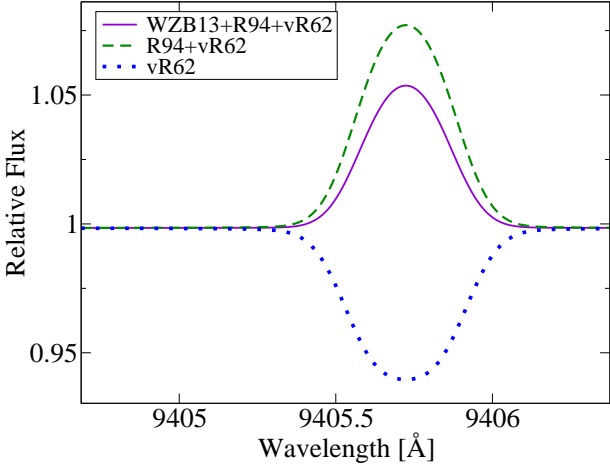


Figure 8. NLTE line profiles of C I 9405 Å in the model 10400/3.5/0 from calculations with collisional data of Wang et al. (2013) where available, Reid (1994), and van Regemorter (1962) (solid curve, WZB13+R94+vR62), collisional data from Reid (1994) for 537 transitions and formula of van Regemorter (1962) for the remaining ones (dashed curve, R94+vR62), and using formula of van Regemorter (1962) only (dotted curve, vR62). Everywhere, $\log \epsilon_C = 8.43$. The theoretical spectra are convolved with an instrumental profile of $R = 65\,000$.

ment abundance determined from the C I absorption lines, a strength of the C I 9405 Å emission was reproduced, when using data of Wang et al. (2013). They were employed everywhere in further stellar abundance analysis.

3.3 Determination of stellar carbon abundances

In this section, we derive the carbon abundances of the selected stars from C I and C II lines using the atomic data from Table 1. The results for individual stars are as follows.

Vega: no emission line of C I is observed in the Vega’s spectrum. For the lines longwards 10480 Å we adopted equivalent widths (EW) from Lambert et al. (1982). All the C I lines can be divided into two groups. Lines in the visible spectral range ($\lambda \leq 7115.2$ Å, 10 lines) are weak, with $EW < 50$ mÅ, while lines in the near-IR spectral range ($10\,123.9$ Å $\leq \lambda \leq 10\,754$ Å, 10 lines) are strong, with $EW > 100$ mÅ. NLTE and LTE abundances from individual lines are presented in Table 4. Everywhere, NLTE leads to strengthened lines, however, the effect is small, with $\Delta_{NLTE} \leq 0.07$ dex by absolute value, for weak lines because they form in deep atmospheric layers. We note a large abundance discrepancy of 0.40 dex between the two weak lines, 4771 and 7113 Å, that cannot be removed by NLTE. A similar difference was also obtained by Przybilla et al. (2001) and Stuerenburg & Holweger (1990).

For strong lines, Δ_{NLTE} varies mainly between -0.28 and -0.64 dex. Applying the treated model atom, we can reconcile the carbon abundance from the three strong ($\log \epsilon_C = 8.34 \pm 0.06$) and 10 weak ($\log \epsilon_C = 8.32 \pm 0.13$) lines, while, in LTE, the IR lines give systematically higher abundances compared with the visible lines. Using EW from Lambert et al. (1982) leads to a large line-to-line scatter of determined abundances, however, the mean NLTE abundance is consistent with that from visible and near-IR lines,

Table 5. Carbon NLTE abundances of Sirius

λ , Å	EW, mÅ	NLTE	LTE	Δ_{NLTE}
C I				
1329.09	} bl	7.90	7.89	+0.01
1329.10				
1329.12				
1329.59	} bl	7.79	7.79	0.00
1329.60				
1459.03	bl	7.84	7.84	0.00
1463.34	bl	7.67	7.66	+0.01
1657.91	bl	7.45	7.44	+0.01
1658.12	bl	7.51	7.50	+0.01
4932.04	bl	7.75	7.74	+0.01
5052.14	6.1	7.69	7.68	+0.01
9088.51	79	7.83	7.88	-0.05
9111.80	92	7.80	7.86	-0.06
9405.73	107	7.49	7.54	-0.05
9658.43	97	7.85	7.96	-0.11
Mean C I		7.71	7.74	
σ		0.15	0.15	
C II				
1335.70	bl	7.64	7.64	0.00
1323.86	} bl	7.74	7.74	0.00
1323.91				
1323.95				
1324.00				
Mean C II		7.69	7.69	
σ		0.15	0.15	
Mean C I+C II		7.71	7.73	
σ		0.14	0.14	

C I 9078, 9088, 9111 Å obtained in this study from analysis of observed spectrum of Vega.

In Table 4 we show also the NLTE abundances derived by Przybilla et al. (2001) and Stuerenburg & Holweger (1990). It is worth noting that their abundances were reduced to the oscillator strengths of Table 1. Our mean NLTE abundance derived from all C I lines, $\log \epsilon_C = 8.34 \pm 0.13$, is consistent with the error bars found in literature. We note, in particular, the C I 9078, 9088, 9111 Å lines, with large departures from LTE, for which the agreement is perfect.

We inspected an impact of varying collisional data on the derived carbon abundances of Vega. In addition to our basic collisional recipe, WZB13+R94+vR62, Table 4 presents the NLTE abundances and abundance corrections for R94+vR62 and vR62, as described above. The abundance difference between WZB13+R94+vR62 and R94+vR62 is small and nowhere exceeds 0.05 dex. However, applying rough theoretical approximations, i.e. the recipe vR62, leads to underestimated NLTE effects, in particular, for the strong lines. For example, the abundance difference between WZB13+R94+vR62 and vR62 amounts to 0.27 dex for C I 10691 Å.

Sirius: the element abundances were derived from the C I and C II lines in a wide spectral region from UV to near-IR (Table 5). The NLTE effects were found to be overall small. For lines of C II and lines of C I in the UV and visible range, $\Delta_{NLTE} \leq 0.01$ dex. This can be easily understood. C II is the dominant ionisation stage. The C I UV lines arise

Table 4. NLTE abundances from C I lines in Vega and NLTE abundance corrections.

λ , Å	WZB13+R94+vR62			R94+vR62	vR62	P2001	SH1990
	NLTE	LTE	Δ_{NLTE}	NLTE / Δ_{NLTE}	NLTE / Δ_{NLTE}	NLTE	NLTE
4771.73	8.52	8.56	-0.04	8.53 / -0.03	8.53 / -0.03	8.38	8.53
4775.89	8.48	8.52	-0.04	8.49 / -0.03	8.50 / -0.02	8.35	
5052.14	8.23	8.27	-0.04	8.24 / -0.03	8.25 / -0.02	8.14	8.23
5380.32	8.28	8.34	-0.06	8.29 / -0.05	8.30 / -0.04	8.19	8.30
6587.61	8.26	8.33	-0.07	8.27 / -0.06	8.28 / -0.05	8.20	
7111.46	8.26	8.32	-0.06	8.27 / -0.05	8.28 / -0.04	8.14	8.24
7113.17	8.12	8.18	-0.06	8.13 / -0.05	8.14 / -0.04	8.03	8.10
7116.98	8.28	8.34	-0.06	8.29 / -0.05	8.30 / -0.04	8.17	8.27
7115.17 } 7115.18 }	8.20	8.26	-0.06	8.21 / -0.05	8.22 / -0.04	8.10	8.28
Mean(vis)	8.32	8.36		8.33	8.34	8.21	8.30
σ	0.13	0.12		0.13	0.13	0.12	0.14
9078.28	8.39	8.84	-0.45	8.39 / -0.45	8.56 / -0.28	8.23	
9088.51	8.35	8.88	-0.53	8.36 / -0.52	8.61 / -0.27	8.40	8.33
9111.80	8.27	8.86	-0.59	8.29 / -0.57	8.49 / -0.37	8.31	8.35
Mean(IR)	8.34	8.86		8.35	8.56	8.32	8.34
σ	0.06	0.02		0.05	0.06	0.09	0.01
Mean(vis+IR)	8.33	8.55		8.34	8.41	8.25	8.31
σ	0.11	0.25		0.11	0.16	0.12	0.11
10123.87	8.10	8.38	-0.28	8.12 / -0.26	8.26 / -0.12		8.21
10683.08	8.45	8.99	-0.54	8.43 / -0.56	8.71 / -0.28		8.45
10685.36	8.62	9.03	-0.41	8.67 / -0.36	8.88 / -0.15		8.56
10691.24	8.26	8.90	-0.64	8.24 / -0.66	8.53 / -0.37		8.36
10729.53	8.16	8.52	-0.36	8.12 / -0.40	8.26 / -0.26		8.22
10707.32	8.32	8.68	-0.36	8.28 / -0.40	8.42 / -0.26		8.33
10753.98	8.35	8.44	-0.09	8.37 / -0.07	8.45 / 0.01		8.33
Mean(all)	8.34	8.65		8.35	8.47	8.25	8.34
σ	0.13	0.28		0.13	0.20	0.12	0.12

Notes: P2001: Przybilla et al. (2001), SH1990: Stuerenburg & Holweger (1990).

in the transitions between the lowest levels, which are closely coupled together (see the departure coefficients in Fig. 3). Both C I visible lines are weak. For C I near-IR lines, the NLTE corrections are negative and do not exceed 0.11 dex in absolute value. The mean NLTE abundances from lines of the two ionization stages, C I and C II, appear to be consistent. Although, we note rather large line-to-line scatter for C I.

Small influence of NLTE on the carbon abundance determination for Sirius makes possible to compare our results with the data obtained by different studies under the LTE assumption. A complete analysis of the literature data was given by Landstreet (2011) who analysed the UV spectrum of Sirius. The average abundance, $\log \epsilon_{\text{C}} = 7.79 \pm 0.18$, deduced by Landstreet (2011) (his Table 1) agrees well with our determination.

For the other five stars of our programme, the abundance results are presented in Table 6. In all stars but the coolest one, HD 73666, few/all C I lines are observed in emission. These lines are marked by 'e' in the corresponding Δ_{NLTE} columns. For comparison, we adopted the solar carbon NLTE abundance, $\log \epsilon_{\text{C}} = 8.43$, derived by Alexeeva & Mashonkina (2015) from the solar C I atomic lines.

HD 73666: there are plenty of C I lines in the spectrum

of this Blue Straggler, while C II is represented by the only weak line. The mean NLTE abundances from lines of the two ionization stages, C I and C II, were found to be consistent, and they are 0.1 dex higher than the solar value, in line with the overall metallicity of HD 73666 (Fossati et al. 2007).

21 Peg: this is the coolest star in our sample that shows an emission in the C I near-IR lines at 8335 Å and 9405 Å. As discussed in Sect. 2.3, the NLTE abundance corrections are positive and large for the C I visible lines, with Δ_{NLTE} up to +0.56 dex. This explains low carbon abundance obtained from these lines by Fossati et al. (2009) under the LTE assumption. We determined the element abundance from the C I emission lines, too, and they appear to be consistent with that from the C I absorption lines. The departures from LTE are minor for C II. NLTE provides consistent abundances from lines of the two ionisation stages, C I and C II, including the C I emission lines, in contrast to LTE, where an abundance difference between the individual lines reaches 0.5 dex and the emission lines cannot be reproduced. The best NLTE fits of the C I absorption and emission lines in 21 Peg are shown in Fig. 7. The obtained carbon NLTE abundance of 21 Peg is close to the solar value.

HD 22136: we could measure only three lines of C I and four lines of C II in this star because of heavy blending the near-IR spectrum by the telluric lines. Element abundance

Table 6. NLTE abundances and abundance corrections for the program stars.

$\lambda, \text{\AA}$	ι Her			π Cet			HD 22136			21 Peg			HD 73666		
	NLTE	LTE	Δ_{NLTE}	NLTE	LTE	Δ_{NLTE}	NLTE	LTE	Δ_{NLTE}	NLTE	LTE	Δ_{NLTE}	NLTE	LTE	Δ_{NLTE}
C I															
6007.17													8.61	8.63	-0.02
6012.22													8.60	8.62	-0.02
6013.21													8.46	8.48	-0.02
6014.83													8.59	8.61	-0.02
7111.46										8.31	8.18	+0.13	8.48	8.54	-0.06
7113.17				8.57	8.14	+0.43				8.23	8.10	+0.13	8.45	8.52	-0.07
7115.17										8.42	8.48	-0.06			
7115.18															
7116.98										8.28	8.15	+0.13	8.58	8.64	-0.06
7119.65										8.35	8.22	+0.13	8.64	8.70	-0.06
4932.04										8.48	8.08	+0.40			
5039.06													8.52	8.50	+0.02
5052.14										8.26	7.81	+0.45	8.53	8.51	+0.02
5380.32										8.22	7.66	+0.56	8.53	8.51	+0.02
4762.52										8.46	8.40	+0.06			
4766.66										8.35	8.29	+0.06			
4770.02										8.49	8.43	+0.06	8.47	8.50	-0.03
4771.73										8.46	8.40	+0.06			
4775.89										8.39	8.33	+0.06	8.72	8.75	-0.03
8335.14	8.37		<i>e</i>	8.49		<i>e</i>	8.44		<i>e</i>	8.22		<i>e</i>	8.71	8.77	-0.06
9061.43	8.36		<i>e</i>							8.35	8.48	-0.13			
9062.49										8.52	8.65	-0.13			
9078.28	8.51		<i>e</i>							8.39	8.46	-0.07			
9088.51	8.34		<i>e</i>				8.51	8.01	+0.50	8.40	8.49	-0.09	8.58	8.90	-0.32
9111.80							8.42	8.07	+0.35	8.44	8.57	-0.13	8.60	8.97	-0.37
9405.73	8.52		<i>e</i>	8.64		<i>e</i>				8.50		<i>e</i>	8.55	8.61	-0.06
9603.02										8.35	8.40	-0.05			
9658.43	8.36		<i>e</i>							8.40	8.54	-0.14	8.61	9.02	-0.41
Mean C I	8.42			8.57	8.14		8.46	8.04		8.38	8.36		8.57	8.63	
σ	0.08			0.08	–		0.05	0.04		0.09	0.26		0.08	0.17	
C II															
3918.97	8.38	8.28	+0.10	8.46	8.44	+0.02	8.36	8.35	+0.01	8.39	8.38	+0.01			
3920.68	8.45	8.35	+0.10												
4267.00	8.33	8.26	+0.07	8.44	8.43	+0.01	8.41	8.40	+0.01	8.35	8.34	+0.01	8.54	8.54	0.00
4267.26				8.44	8.43	+0.01				8.36	8.35	+0.01			
6578.05	8.71	9.13	-0.42	8.50	8.50	0.00	8.39	8.44	-0.05	8.35	8.36	-0.01			
6582.88	8.55	8.97	-0.42	8.54	8.54	0.00	8.49	8.54	-0.05	8.41	8.42	-0.01			
5132.95	8.38	8.46	-0.08												
5133.28	8.37	8.45	-0.08												
5137.25	8.43	8.51	-0.08												
5139.17	8.35	8.43	-0.08												
5143.49	8.38	8.45	-0.07												
5145.16	8.41	8.48	-0.07	8.37	8.40	-0.03									
5151.09	8.36	8.42	-0.06												
7231.33	8.29	8.18	+0.11												
7236.41				8.38	8.35	+0.03									
7237.17	8.41	8.34	+0.07	8.37	8.34	+0.03									
Mean C II	8.43	8.58		8.44	8.45		8.42	8.44		8.37	8.37		8.54	8.54	
σ	0.10	0.26		0.06	0.07		0.03	0.08		0.03	0.03		–	–	
Mean	8.43	8.58		8.45	8.41		8.43	8.34		8.38	8.36		8.57	8.62	
σ	0.10	0.26		0.09	0.11		0.05	0.21		0.09	0.23		0.08	0.16	

Notes. Emission lines are marked by symbol *e*.

derived from the C I 9405 Å emission line is consistent with the NLTE abundances from the C I and C II absorption lines. The obtained carbon NLTE abundance of HD 22136 is very similar to the solar one.

π Cet: this star is hotter by 100 K than HD 22136 and slightly faster rotating. Two emission lines, C I 8335 and 9405 Å, were detected in its spectrum. The only measurable absorption line of C I is 7113 Å. NLTE abundance corrections for the C II lines are mainly positive and, for each line, Δ_{NLTE} does not exceed 0.03 dex in absolute value. Carbon abundances from the absorption and emission lines of C I agree with each other, but an average abundance from the C I lines is higher than that derived from the C II lines, although a difference of 0.13 dex is still within 2σ .

ι Her: this is the hottest star of our sample. No C I line was detected in the visible range. All the C I near-IR lines appear in emission. NLTE abundance corrections have different sign for different lines of C II. For most lines they do not exceed 0.11 dex in absolute value, but they are large and negative, with $\Delta_{\text{NLTE}} = -0.42$ dex, for strong C II 6578, 6582 Å lines. Our NLTE analysis provides consistent abundances from different groups of lines, i.e. the C I emission lines and C II absorption lines. The best NLTE fits of the C I emission lines and C II absorption lines are shown in Fig. 7. The obtained carbon abundance of ι Her, $\log \epsilon_{\text{C}} = 8.43 \pm 0.10$, is essentially solar. Similar result, $\log \epsilon_{\text{C}} = 8.40 \pm 0.07$, was obtained by Nieva & Przybilla (2012) in their NLTE analysis of the C II lines in ι Her. Larger dispersion in our abundance determination is mainly caused by the two lines, C II 6578 Å and 6582 Å, which give about 0.2 dex higher abundance compared with that from the remaining lines, while no significant abundance discrepancy between different lines was obtained by Nieva & Przybilla (2012).

4 CONCLUSIONS

The motivation of this work was to solve two problems in stellar astrophysics: the search for explanation of the appearance of emission lines in C I in the near-IR spectral region and a reliable determination of carbon abundances for AB-type stars. We constructed a comprehensive model atom for C I – C II using the most up-to-date atomic data and evaluated the NLTE line formation for C I and C II in classical 1D models representing the atmospheres of A and late B-type stars.

Our NLTE calculations predict that some lines of C I in the near IR spectral range may appear as emission lines depending on the atmospheric parameters. The emission appears first in the C I 8335 Å and 9405 Å singlet lines at effective temperature of 9250 K to 10 500 K depending on the value of $\log g$. It is strengthened toward higher T_{eff} , reaches a maximal level at $T_{\text{eff}} = 16\,000$ K ($\log g = 3$) and almost disappears at $T_{\text{eff}} = 22\,000$ K. The C I triplet lines at 9061–9111 Å and 9603–9658 Å come into emission at $T_{\text{eff}} > 15\,000$ K ($\log g = 4$). The mechanisms driving the C I emission can be understood as follows. A prerequisite of the emission phenomenon is the overionization-recombination mechanism resulting in a depopulation of the lower levels of C I to a greater extent than the upper levels. Extra depopulation of $3s^1P^\circ$ and $3s^3P^\circ$, which are the lower levels of the transitions corresponding to the listed near-IR lines, can be

caused by photon loss in the UV lines C I 2479, 1930, and 1657 Å. In the models with T_{eff} of about 10 000 K only, C I 2479 Å plays a role draining population of the $3s^1P^\circ$ singlet level effectively in the layers, where the C I 8335 and 9405 Å lines form, while these layers are optically thick for radiation at 1930 and 1657 Å. With increasing T_{eff} , formation depths of all the C I UV lines shift inwards, resulting in a depopulation of not only $3s^1P^\circ$, but also $3s^3P^\circ$ and the lower levels of the emission triplet lines at 9061 – 9111 Å and 9603 – 9658 Å.

Our theoretical results were confirmed with observations of the reference stars. The stellar sample consists of seven bright and apparently slow-rotating A- and late B-type stars in the solar neighbourhood. Our analysis is based on high S/N and high-resolution spectra with a broad wavelength coverage.

The C I emission lines were measured in the four hottest stars, with $T_{\text{eff}} \geq 10\,400$ K, and they were well reproduced in our NLTE calculations. For each star, the mean NLTE abundances from lines of the two ionisation stages, C I and C II, including the C I emission lines, were found to be consistent. Thus, we settled the dispute on whether the C I emission in the late-B stars is produced by the circumstellar disc, or vertical stratification / horizontal inhomogeneity of the atmosphere, or the NLTE effects in the atmosphere.

The six of our stars reveal highly uniform and close-to-solar carbon abundance. We confirm a significant underabundance of carbon in Sirius, with $[C/H] = -0.72$.

We show an importance of applying accurate atomic data to the statistical equilibrium calculations. In particular, the C I emission phenomenon turns out to be extremely sensitive to varying electron-impact excitation rates. If the latter are not accounted for properly, the stellar C I emission lines cannot be reproduced. The results obtained in this study favour the collisional data for C I from predictions of Wang et al. (2013).

It is worth noting, WELs of Mg II, Si II, P II, Ca II, Cr II, Fe II, Ni II, Cu II, and Hg II were detected in the near-UV and visible spectral regions for several stars not showing any trace of chromosphere (Sigut et al. 2000, Wahlgren & Hubrig 2000, 2004, Castelli & Hubrig 2007). According to Wahlgren (2008), WELs of some metals are observed in sharp-lined spectra of mid- to late-B type stars. The WELs are detected over a range of element abundance and are found among both chemically-normal and chemically-peculiar stars. The NLTE line-formation calculations for these specific ions are highly desirable to understand mechanisms of the observed emission.

Acknowledgements. This research is based on observations obtained with MegaPrime/MegaCam, a joint project of CFHT and CEA/IRFU, at the Canada–France–Hawaii Telescope (CFHT) which is operated by the National Research Council (NRC) of Canada, the Institut National des Sciences de l’Univers of the Centre National de la Recherche Scientifique (CNRS) of France, and the University of Hawaii. We thank Oleg Zatsarinny for providing us the data on effective collision strengths for the C I transitions published in Wang et al. (2013). This work was supported in part by the Russian Foundation for Basic Research (grants 16-32-00695 and 15-02-06046).

REFERENCES

- Alexeeva S. A., Mashonkina L. I., 2015, *MNRAS*, 453, 1619
- Bailey J. D., Landstreet J. D., 2013, *A&A*, 551, A30
- Burkhart C., Coupry M. F., 1998, *A&A*, 338, 1073
- Butler K., Giddings J., 1985, Newsletter on the analysis of astronomical spectra, No. 9, University of London
- Carlsson M., Rutten R. J., Shchukina N. G., 1992, *A&A*, 253, 567
- Castelli F., Hubrig S., 2007, *A&A*, 475, 1041
- Cunto W., Mendoza C., Oechsenbein F., Zeippen C. J., 1993, Bulletin d'Information du Centre de Donnees Stellaires, 42, 39
- Fossati L., Bagnulo S., Monier R., Khan S. A., Kochukhov O., Landstreet J., Wade G., Weiss W., 2007, *A&A*, 476, 911
- Fossati L., Ryabchikova T., Bagnulo S., Alecian E., Grunhut J., Kochukhov O., Wade G., 2009, *A&A*, 503, 945
- Hibbert A., Biemont E., Godefroid M., Vaecq N., 1993, *A&AS*, 99, 179
- Hill G., Gulliver A. F., Adelman S. J., 2010, *ApJ*, 712, 250
- Hill G. M., Landstreet J. D., 1993, *A&A*, 276, 142
- Kochukhov O., , 2010, <http://www.astro.uu.se/oleg/binmag.html>
- Kupka F., Piskunov N., Ryabchikova T. A., Stempels H. C., Weiss W. W., 1999, *A&AS*, 138, 119
- Lambert D. L., Roby S. W., Bell R. A., 1982, *ApJ*, 254, 663
- Landstreet J. D., 2011, *A&A*, 528, A132
- Leonard P. J. T., 1996, in Milone E. F., Mermilliod J.-C., eds, *The Origins, Evolution, and Destinies of Binary Stars in Clusters Vol. 90 of Astronomical Society of the Pacific Conference Series, Blue Stragglers in Star Clusters*. p. 337
- Luo D., Pradhan A. K., Saraph H. E., Storey P. J., Yu Y., 1989, *Journal of Physics B Atomic Molecular Physics*, 22, 389
- Malfait K., Bogaert E., Waelkens C., 1998, *A&A*, 331, 211
- Nieva M. F., Przybilla N., 2008, *A&A*, 481, 199
- Nieva M.-F., Przybilla N., 2012, *A&A*, 539, A143
- Przybilla N., Butler K., Becker S. R., Kudritzki R. P., Venn K. A., 2000, *A&A*, 359, 1085
- Przybilla N., Butler K., Kudritzki R. P., 2001, *A&A*, 379, 936
- Przybilla N., Nieva M.-F., Butler K., 2011, *Journal of Physics Conference Series*, 328, 012015
- Ralchenko Y. A., Kramida E., Reader J., Team N. A., 2008, *NIST Atomic Spectra Database (version 3.1.5)*. USA
- Reid R. H. G., , 1994, Electron impact excitation of C I
- Rentzsch-Holm I., 1996, *A&A*, 312, 966
- Roby S. W., Lambert D. L., 1990, *ApJS*, 73, 67
- Ryabchikova T., Piskunov N., Pakhomov Y., Tsymbal V., Titarenko A., Sitnova T., Alexeeva S., Fossati L., Mashonkina L., 2016, *MNRAS*, 456, 1221
- Rybicki G. B., Hummer D. G., 1991, *A&A*, 245, 171
- Sadakane K., 1981, *PASP*, 93, 587
- Seaton M. J., 1962, *Proceedings of the Physical Society*, 79, 1105
- Shulyak D., Tsymbal V., Ryabchikova T., Stütz C., Weiss W. W., 2004, *A&A*, 428, 993
- Sigut T. A. A., 2001, *A&A*, 377, L27
- Sigut T. A. A., Landstreet J. D., Shorlin S. L. S., 2000, *ApJ*, 530, L89
- Smith K. C., Dworetzky M. M., 1993, *A&A*, 274, 335
- Stuerenburg S., Holweger H., 1990, *A&A*, 237, 125
- van Regemorter H., 1962, *ApJ*, 136, 906
- Venn K. A., Lambert D. L., 1990, *ApJ*, 363, 234
- Wahlgren G. M., 2008, *Contributions of the Astronomical Observatory Skalnaté Pleso*, 38, 279
- Wahlgren G. M., Hubrig S., 2000, *A&A*, 362, L13
- Wahlgren G. M., Hubrig S., 2004, *A&A*, 418, 1073
- Wang Y., Zatsarinny O., Bartschat K., 2013, *Phys. Rev. A*, 87, 012704
- Wilson N. J., Bell K. L., Hudson C. E., 2005, *A&A*, 432, 731